RSC Advances

PAPER

View Article Online
View Journal | View Issue

Cite this: *RSC Adv.*, 2025, **15**, 19132

Innovative and sustainable synthesis of biogenic gold nanoparticles for cholesterol detection: gelatine role in enhanced stability and catalytic activity†

Thi Lan Huong Nguyen,[a] Ngoc Vy Nguyen,[b] Van Dat Doan,[b] Thi Dung Nguyen,[c] Anh Tien Nguyen,[d] Thi Long Do,[b] Renat Maratovich Akhmadullin[e] and Hien Y Hoang *[fg]

The biosynthesis of metal nanoparticles using natural extracts represents a significant advancement in quantitative analysis, as it effectively reduces nanoparticle aggregation, thereby enhancing the precision and dependability of analytical results. However, particle agglomeration of the nanoparticles continues to be a notable hurdle. In this study, for the first time, we addressed this issue by introducing gelatine into the synthesis of biogenic gold nanoparticles (AuNPs). Interestingly, although gelatine exhibits reducing properties, its primary role in this context is as an agglomeration inhibitor when combined with the natural extract. Analyses including SEM-EDS, element mapping, TEM, XRD, FT-IR, DLS, TGA-DTG, and zeta potential revealed that the incorporation of gelatine alters the morphology of biogenic AuNPs, promoting resistance to aggregation. The synthesized AuNPs have exhibited a dual-layer structure, with coatings consisting of both natural extract and gelatine. Additionally, the gelatine presence marginally enhances the intrinsic catalytic activity of AuNPs. Importantly, the gelatine coating does not compromise the efficacy of AuNPs in the colorimetric assay, partially in cholesterol detection, which demonstrated a wide-ranging detection capability of 1–1000 μM with an LOD of 3.48 μM. Furthermore, the analytical accuracy was validated using CG-FID, achieving near-perfect results in fast food samples such as snack-sticks and butter & pork floss baguettes. Hopefully, these findings in this study will not only contribute to advancements in the field of quantitative analysis but also provide valuable insights for various industries seeking sustainable methodologies for the synthesis of metallic nanoparticles.

Received 3rd February 2025
Accepted 30th May 2025

DOI: 10.1039/d5ra00798d

rsc.li/rsc-advances

1. Introduction

In the ever-evolving landscape of modern industry, the relentless pursuit of quality and safety in food products has become a top priority. As such, the demand for rigorous analytical methodologies within food analysis laboratories has surged to ensure that food components meet stringent regulatory standards.

Cholesterol, a crucial component in the human body's biochemical processes, arises through two pathways: endogenous synthesis and dietary intake. Serving as a precursor for steroid hormone synthesis and aiding in the regulation of vital bodily functions, cholesterol also contributes to the synthesis of cortisol, which modulates blood glucose levels.[1] However, regularly consuming large amounts of cholesterol-rich foods, such as fast foods, can contribute to high blood cholesterol levels, posing a significant risk factor for atherosclerosis and various cardiovascular complications.[2] Thus, meticulous control of cholesterol levels in food products is imperative to safeguard public health.

Various analytical methods, including chromatography, spectroscopy, and electrochemistry, have been utilized for cholesterol analysis.[3–6] Each method presents its unique strengths and weaknesses. Chromatography offers excellent selectivity; however, its expensive instrumentation and intricate sample preparation process are notable drawbacks. Similarly,

[a]*Institute of Biotechnology and Food Technology, Industrial University of Ho Chi Minh City, Ho Chi Minh City, 700000, Vietnam*

[b]*Faculty of Chemical Engineering, Industrial University of Ho Chi Minh City, Ho Chi Minh City, 700000, Vietnam*

[c]*Biotechnology Center of Ho Chi Minh City, Ho Chi Minh City, 700000, Vietnam*

[d]*Faculty of Chemistry, Ho Chi Minh City University of Education, 280 An Duong Vuong, Ho Chi Minh City, 700000, Vietnam*

[e]*R&D "AhmadullinS" LLC, 34 Syberian Tract, Kazan, 420139, Russia*

[f]*Center for Advanced Chemistry, Institute of Research & Development, Duy Tan University, 03 Quang Trung, Danang City, 550000, Vietnam. E-mail: hoanghieny@duytan.edu.vn*

[g]*Faculty of Natural Sciences, Duy Tan University, 03 Quang Trung, Da Nang, 550000, Vietnam*

† Electronic supplementary information (ESI) available. See DOI: https://doi.org/10.1039/d5ra00798d

electrochemistry boasts an extensive linear detection range with exceptional sensitivity, yet the labour-intensive electrode modification process remains a concern. On the other hand, colorimetry stands out for its simplicity, rapid response, and minimal reliance on expensive instrumentation. The advantages of colorimetric assay offer a promising alternative to complex analytical methods, especially in point-of-care testing and field applications. The operational simplicity of colorimetry allows for easy handling by non-specialists. The colorimetric paper-based sensors such as dipsticks proved to be user-friedly by integrating sample transport and reaction zones onto a simple, disposable platform.[7,8] The use of widely available and low-cost materials such as paper and cellulose substrates, combinned with a less demanding fabrication processes compared to manufacturing microelectronic or complex optical sensors, makes the colorimetric sensing approach a cost-effective alternative.[9] Additionally, the minimal requirement for costly readout instruments greatly reduces the overall assay cost. Moreover, the ability to deliver results within minutes without external power or equipment makes colorimetry ideal for resource-limited settings and real-time screening – an advantage that many modern analytical techniques are unable to offer.

However, in comparison to alternative analytical techniques, colorimetric analysis may exhibit slightly lower sensitivity.[10] Amidst this backdrop, the emergence of nanotechnology and nanomaterials has revolutionized analytical chemistry, offering novel avenues for sensitive and selective detection of various compounds. The colorimetric sensors based on localized surface plasmon resonance (LSPR) take advantage of the strong light absorption of noble metal nanoparticles, while nanozymes enhance signals through catalytic reactions.[11] These enhancements allow the colorimetric assay to detect certain analytes at very low concentrations, down to the nanomolar or even picomolar range, comparable to those attained by fluorescence, and electrochemical method.

Noble metal nanoparticles, especially gold nanoparticles (AuNPs), are highly regarded for their unique optical properties and SPR effects.[12] These properties make them ideal candidates for the fabrication of biosensors and chemical sensors with unparalleled sensitivity and specificity.[13,14] Specifically, AuNPs are recognized as the most potent among the metallic nanoparticles[15] and showing excellent peroxidase-mimicking properties and playing a key role in cholesterol detection.[16,17] Amid the rise of modern digital technologies, the colorimetric AuNPs-based sensors have been developed to quantificate cholesterol content *via* smartphone-assisted applications, demonstrating high accuracy equivalent to clinically observed values. These advancements indicate that colorimetric method is progressively closing the gap in measurement efficiency and accuracy when compared to other modern analytical techniques.[18] However, in many instances, AuNPs are employed as standalone entities within detection systems, leading to potential issues such as aggregation, which ultimately impede their catalytic efficiency towards H_2O_2.[1]

The utilization of plant extract in the synthesis of metallic nanoparticles is proposed to partly mitigate aggregation phenomenon, yielding multiple benefits, particularly when phytochemicals in this natural extract serve all three roles in facilitating metal ion reduction, nanoparticle formation, and stabilization.[19–21] This approach is regarded as a contemporary trend in AuNPs synthesis, distinguished by its environmental sustainability and efficiency. Consequently, the scientists continue to explore various natural extracts employed in the AuNPs phytosynthesis, sometimes overlooking the quest for an optimal approach to augment the stability of metallic nanoparticles further.[22] The use of natural extract undoubtedly provides notable benefits for metal nanoparticle synthesis. However, it is undeniable that the occurrence of agglomeration during the process remains practically inevitable, highlighting the need for innovative approaches to optimize extract usage in synthesizing metallic nanoparticles. In another aspect, gelatine, a natural polymer with functional groups analogous to those of extract phytochemicals, is expected to play an important role in mitigating agglomeration during nanoparticle synthesis.[23–25] Its fixed composition, in contrast to the variable nature of the extract depending on the plant source, offers a consistent advantage as an additive. Moreover, gelatine has been used in recent studies[26–29] for AuNPs synthesis, further supporting its potential role. Typically, Vo and co-workers successfully synthesized dendritic and branched AuNPs using gelatine as an agent with both reducing and stabilizing properties; however, the specific applications of nanoparticles remain unexplored.[29] In a study outside the field of colorimetric analysis,[26] Chen *et al.* utilized nanogel derived from gelatine and protein as a stabilizing reductant for the synthesis of AuNPs exhibiting metal-enhanced luminescence/fluorescence. Similarly, Zhang's group employed gelatine to synthesize AuNPs for applications in cytosensing and drug uptake.[27] The aforementioned examples demonstrate that gelatine plays a dual-function agent for reduction and stabilization, not only in quantitative analysis but also across various other fields. However, its primary function in the AuNPs synthesis remains unexplored. Additionally, no studies have investigated the use of stabilizers, such as gelatine, in the biogenic AuNPs synthesis or its potential influence on the formation and catalytic activity of the nanoparticles. These gaps in knowledge have motivated us to undertake this study.

Here, we report the first successful incorporation of gelatine with natural extract to enable a one-pot *in situ* synthesis of AuNPs. The study focuses on elucidating the role of gelatine when incorporated into the synthesis process and to evaluate the catalytic properties of the nanoparticles obtained.

Prior to accomplishing this objective, the initial step involves selecting an appropriate natural extract and synthesis method that aligns with the current trend of sustainable development. It is worth noting that some studies even used extracts that have yet to undergo toxicity evaluation in AuNP synthesis, thereby introducing potential hazards into the synthesis process.[30] Therefore, we prioritize selecting a non-toxic extract that has a proven history of safe use in daily life. *Stachys affinis* (SA) extract, widely utilized in traditional medicines and consumed as both edible plants and food additives in various cultures, offers abundant bioactive compounds such as flavonoids,

phenolics, and terpenoids, making it an excellent candidate for the phytosynthesis of AuNPs.[31] The complexity and high cost of the traditional synthesis method prompted us to synthesize AuNPs by the one-pot *in situ* method in this study. After the synthesis process, we initially conducted the comparative analysis of morphological characterizations and peroxidase-like activity of the as-synthesized AuNPs (denoted as gelatine/SA@AuNPs) with that of AuNPs synthesized solely using SA extract (abbreviated as SA@AuNPs). Analyses including SEM-EDS, element mapping, TEM, XRD, FT-IR, DLS, TGA-DTG, and zeta potential confirmed that the incorporation of gelatine in the synthesis process altered the morphology of the formed AuNPs effectively preventing agglomeration and slightly enhancing its catalytic performance. Interestingly, while previous studies reported that gelatine could act as a reductant during the nanoparticle synthesis, our results suggest that, in combination with SA extract, gelatine primarily served as encapsulating and stabilizing agent, with SA extract assuming the primary role in reduction. The optimal conditions of the gelatine/SA@AuNPs synthesis were further studied to refine the proposed methodology. Afterwards, the gelatine@AuNPs was further utilized to develop an effective biosensor strip designed for the colorimetric cholesterol quantification, employing 3,3′,5,5′-tetramethylbenzidine (TMB) as a reliable substrate. Given the unique properties of gelatine, such as its biocompatibility, biodegradability, ability to form stable matrices, and cost-effectiveness, its application as a supportive material holds promise in enhancing the stability and catalytic efficiency of AuNPs, thereby improving the sensitivity and selectivity of the cholesterol detection platform. Additionally, we extended our investigation to the practical application of the as-synthesized catalyst for detecting cholesterol in real food samples, and the obtained results were cross-checked with capillary gas chromatography with flame ionization detection (CG-FID) measurements to assess the practical applicability of the targeted catalyst.

Through this comprehensive analysis, we aim to introduce an efficient approach to enhance the efficiency of metallic nanoparticle synthesis, thereby contributing to the advancement of biosensing technologies for sensitive, and reliable detection in various applications, ultimately benefiting public health and safety.

2. Materials and methods

2.1. Materials and analytical equipment

The SA roots were sourced from the Biotechnology Center of Ho Chi Minh City (2374 QL1A, Ward 2, District 12, Ho Chi Minh City). Chemicals utilized in the experiment comprised 3,3′,5,5′-tetramethylbenzidine, sodium hydroxide (NaOH), chloroauric acid ($HAuCl_4 \cdot 3H_2O$) hydrogen peroxide (H_2O_2), cholesterol ($C_{27}H_{46}O$), cholesterol oxidase (ChOx), sodium acetate (CH_3COONa), acetic acid (CH_3COOH), zinc chloride ($ZnCl_2$), niacin (C_5H_4NCOOH), uric acid ($C_5H_4N_4O_3$), ascorbic acid ($C_6H_8O_6$), magnesium chloride hexahydrate ($MgCl_2 \cdot 6H_2O$), glycine ($C_2H_5NO_2$), tryptophan ($C_{11}H_{12}N_2O_2$), sodium chloride (NaCl), riboflavin ($C_{17}H_{20}N_4O_6$), and glucose ($C_6H_{12}O_6$), all purchased from Sigma Aldrich & Co., Inc. Each chemical was of analytical grade purity to guarantee the accuracy and dependability of the experimental outcomes.

X-ray diffraction (XRD) patterns were collected using an XRD-6100 instrument from SHIMADZU for structural characterization. Thermal stability was evaluated using thermogravimetric analysis (TGA) performed on a Thermal Analysis System TGA/DSC 3+ (Mettler Toledo – Switzerland). Particle size distribution and zeta potential were measured using a Horiba SZ-100 instrument (Japan) to assess colloidal properties. The morphology and size were examined using a Hitachi S-4800 field emission scanning electron microscope (FE-SEM) and a high-resolution transmission electron microscope (HR-TEM, JEM-2100, JEOL). Fourier-transform infrared (FTIR) spectra were obtained using a Bruker Equinox 55 spectrophotometer (Germany) to analyse chemical compositions. UV-vis spectroscopy was conducted with a Cary 60 UV-vis spectrophotometer (Agilent, USA) to examine the optical properties. The obtained results are presented as the mean ± standard deviation. Statistical analysis was carried out using ANOVA, and differences were considered significant at $p < 0.05$.

2.2. Extract preparation

The SA roots were peeled and thinly sliced, then washed thoroughly with water twice to remove external impurities. Subsequently, the sliced roots were chopped into smaller pieces and dried at 70 °C until completely dry. The dried roots were then finely ground, and the ratio of solvent to SA mass was determined prior to subsequent experimentation. The SA roots were subjected to extraction using an ultrasonic bath to obtain the extract. The extraction process lasted for 3 h, with the temperature maintained at a stable 80 °C throughout. The resulting extract was passed through filter paper to remove solid residues. To ensure preservation, the extract should be stored at a temperature of 3–5 °C and utilized within 3–5 days of preparation to maintain its efficacy.

2.3. Gelatine/SA@AuNPs synthesis

The spontaneous *in situ* synthesis of gelatine@AuNPs was achieved by mixing gelatine with $HAuCl_4$ and SA extract, as described in Fig. 1a. The synthesis reaction was initiated by slowly adding the 2.5 mL of 5% gelatine solution into 10 mL of 0.5 mM $HAuCl_4$ solution under constant agitation for 15 min. This mixture was then heated to 70 °C and supplemented with 5 mL of SA extract. The reaction was maintained for approximately 50 min to facilitate the favourable reduction of Au^{3+} ions to AuNPs by the bioactive molecules present in the SA extract. A shift in solution color from pale yellow to dark purple was observed, confirming the formation of AuNPs. Upon completion of the reaction, the gelatine/SA@AuNPs were washed multiple times and separated from the supernatant by centrifugation to eliminate unreacted Au^{3+} ions or unbound AuNPs. Additionally, for comparative purposes, the traditional biogenic AuNPs were synthesized using the same procedure but without the addition of gelatine. To examine the effect of gelatine

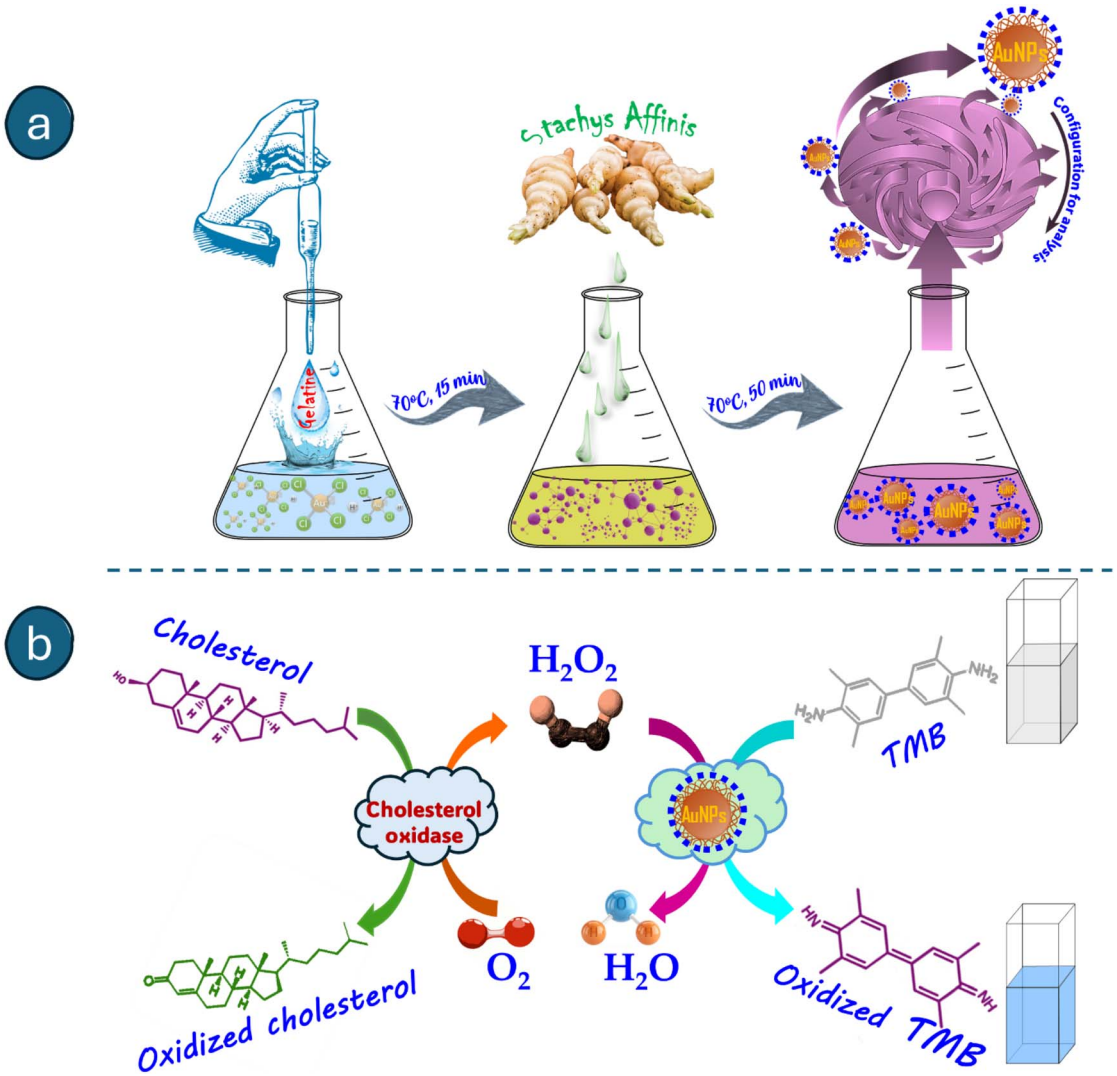

Fig. 1 Diagrammatic representation of the gelatine/SA@AuNPs synthesis (a), the mechanistic explanation of cholesterol detection *via* colorimetry (b).

concentration on the particle size of the synthesized nanoparticles, its concentration was adjusted between 1% and 7.5%.

2.4. Peroxidase-mimicking activity

The peroxidase-like efficiency of the catalyst was evaluated using a colorimetric assay with TMB as the substrate, in which the targeted catalyst facilitated the oxidation of TMB by H_2O_2. Briefly, a reaction mixture containing 300 μL of 400 μM H_2O_2, 1000 μL of acetate buffer (pH 5), and 200 μL of 5 mM TMB was prepared and incubated with 60 μL of gelatine/SA@AuNPs nanocomposite. The development of a blue colour, indicative of oxidized TMB, was monitored by measuring the absorbance at 652 nm. A series of H_2O_2 concentrations (1–2000 μM) was tested to investigate the concentration-dependent response and sensitivity of the nanocomposite. A calibration curve was constructed by plotting the absorbance values against the corresponding H_2O_2 concentrations.

2.5. Cholesterol detection assay

The cholesterol detection assay utilized the gelatine/SA@AuNPs composite as the sensing platform. In this assay, the biogenic nanoparticles catalyze the colorimetric TMB oxidation by H_2O_2, which is generated during the cholesterol oxidation in the presence of cholesterol oxidase (Fig. 1b). The colour intensity increase in TMB solution provides the foundation for quantifying cholesterol. Initially, a series of cholesterol standard solutions with known concentrations were prepared using a solvent mixture of iso-octane and 1% Triton (v : v = 1 : 1). For each assay, 5 μL of 5 μM cholesterol oxidase, 200 μL of cholesterol solution at varying concentrations, 1000 μL of acetate buffer (pH 5), 200 μL of 5 mM TMB, and 60 μL of gelatine/SA@AuNPs were combined. After being incubated at 50 °C for 30 minutes, the reaction mixture's absorbance was analyzed using a UV-vis spectrophotometer. The cholesterol concentration in the samples was determined based on a calibration curve constructed using the absorbance values obtained from

the standard solutions. The LOD value and the linear range of the assay were determined from the calibration curve. Additionally, the specificity and selectivity of the assay were evaluated by testing the cholesterol concentration in the presence of other interfering substances (1 mM of $ZnCl_2$, $MgCl_2$, uric acid, tryptophan, riboflavin, ascorbic acid, glucose, and glycine) commonly found in food samples.

2.6. Cholesterol detection in real-world samples

Detection of cholesterol in real-world samples involved the analysis of two types of food products: snacks-sticks and butter & pork floss baguettes, procured from VinMart – a chain of convenience supermarkets of Vingroup JSC (District 12, Ho Chi Minh City). The snack is imported from Thailand, while the baguette is manufactured in Vietnam by reputable manufacturers within the supply industry. The ingredients of these fast foods as declared by the manufacturers are presented in Table S1 of ESI.† The sample processing procedure was performed following a previously established protocol.[32] Three random samples of each food type were collected, thoroughly mixed, and ground into fine powder. Subsequently, each 2 g sample was dissolved in 10 mL of KOH/EtOH, then 10 mL of distilled water and 20 mL of *n*-hexane were added. The resulting mixture was incubated in a water bath at 70 °C for 1 h, then centrifuged at 8000 rpm for 5 min. The solid residue was dried by blowing liquid nitrogen, followed by dissolution in isopropanol and 1% Triton (v/v = 1 : 1). The cholesterol content in the samples was quantified according to the procedure outlined above. Besides that, CG-FID measurement was used to assess the accuracy of the obtained results.

3. Results and discussion

3.1. Comparative characteristics

As we predicted, the presence of gelatine in the phytosynthesis of AuNPs substantially alters their morphology, favouring characteristics conducive to the activity of nanoparticles. From the SEM image (Fig. 2a), it is evident that the distribution of metallic nanoparticles in gelatine/SA@AuNPs colloid is uniform. In contrast, the nanoparticle component in the biogenic SA@AuNPs colloid (Fig. 2b) displays heterogeneous dispersion and tends to aggregate into clusters. The analysis result of element mapping further corroborated this observation: while the typical blue spots of AuNPs exhibit homogeneous distribution in the case of gelatine/SA@AuNPs, the opposite was observed in the SA@AuNPs colloid. The EDS analysis also indicates a clear difference in AuNP components in these aforementioned composites. Upon further analysis in the nanoscale, it was discerned for TEM images that using SA extract as a reducing agent prompted the generation of anisotropic AuNPs with irregular shapes such as spheres, triangles, hexagons, cubes, rods, and polygons. These shapes with face-centered structures exhibit characteristic (111), (200), (220), and (311) lattice planes, as revealed in XRD analysis (Fig. S1†), which are in agreement with the standard card ICDD No. 04-0784. The formation of anisotropic nanoparticles is easily explained by the ubiquity of SA extract, which comprises multiple reducing agents, such as flavonoids, phenolics, and terpenoids that significantly change the conventional mechanism of nanoparticle growth, thereby leading to anisotropy. Accordingly, in the simultaneous use of multiple reducing agents, initially, the nucleation stage is facilitated by the more powerful reductants, followed by the facilitation of structural formation of nanoparticles by the weaker reductants.[33] The TEM image of SA@AuNPs colloid (Fig. 2d) also indicates that various shapes of the nanoparticles tend to aggregate, with smaller sizes typically associated with spherical, while larger sizes tend to adopt other geometrical morphology, such as hexagons, pentagons, and triangles. The insufficiency of biochemicals responsible for capping and stabilizing the generated AuNPs has been identified as the underlying cause of this phenomenon, as documented in numerous prior studies.[34–36] It is expected that the introduction of gelatine in the synthetic mixture leads to the disappearance of the large anisotropic nanoparticles and a reduction in particle size (Fig. 2c).

As indicated by the size distribution analysis, the majority of nanoparticles in gelatine/SA@AuNPs exhibit sizes below 10 nm, whereas the opposite trend is observed for SA/AuNPs colloid. The trend observed is consistent with the findings from DLS analysis, which indicates the hydrodynamic diameter of nanoparticles in gelatine/SA@AuNPs fall within the range of 72.87–402.44 nm, mostly from 93.02 to 151.57 nm, constituting 53.82% of the total number of particles. For SA@AuNPs, the distribution of hydrodynamic diameter extends up to 4091.63 nm, with the majority falling between 93.02 and 580.41 nm, constituting 71.42% of the total particle. The obtained results highlight the efficacy of gelatine as a potent capping and stabilizing agent during the AuNPs synthesis. Nitrogen-containing component in gelatine plays a pivotal role in achieving such effectiveness.[25] Positively charged amine groups of gelatine, during the ionization process in aqueous solution, can undergo electrostatic adsorption onto the surface of negatively charged AuNPs, thereby forming a hydrophilic coating surrounding AuNPs. This hydrophilic layer acts as a barrier, inhibiting aggregation in the synthesis process and facilitating the uniform dispersion of AuNPs within the aqueous solution, as clearly shown in SEM and TEM analysis. It is therefore unsurprising that upon the addition of gelatine to the synthetic reaction mixture, the zeta potential (ξ), indicative of the aggregative stability of nanodispersion, increases by nearly threefold ($\xi = 18.6$ mV) (Fig. 3a), and considerably exceeds those of AuNPs synthesized from natural extracts (as presented in Table S2†). The presence of this layer had led to the above observation that the particle size of AuNPs, as measured in the DLS analysis (119.33 nm in average), is significantly larger than that (15.12 nm in average) indicated by TEM and XRD analysis.

The FT-IR analysis partially demonstrated the existence of hydrophilic coating layers on both resulting AuNPs samples, evident from the appearance of characteristic vibrations associated with the functional groups of hydrophilic organics present in the spectral analysis of these metallic nanoparticles (Fig. 3b). Specifically, the typical peaks centered at around 3856–3074, 2970–2832, 1711, 1625, 1528, 1382, 1264, 1158, 1058

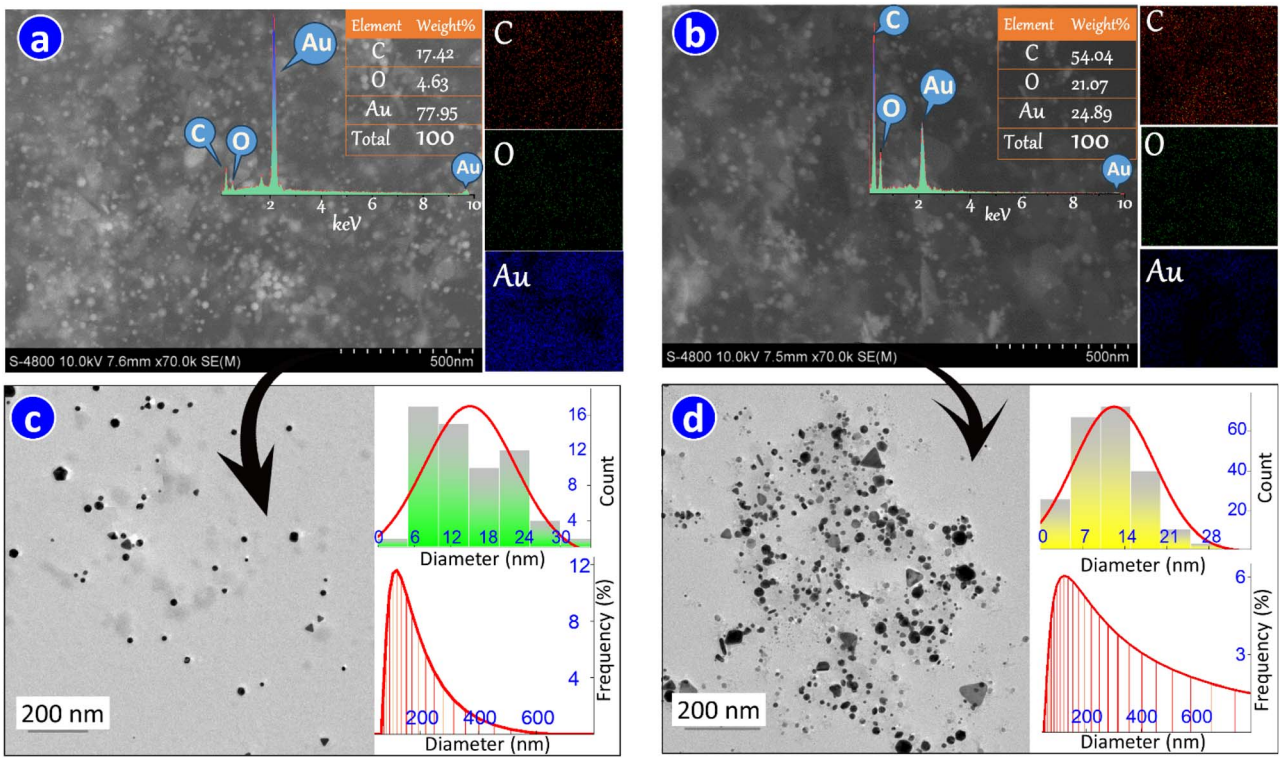

Fig. 2 SEM-EDS images of gelatine/SA@AuNPs (a) and SA@AuNPs (b) (embed images illustrate the elemental mapping), and TEM images of gelatine/SA@AuNps (c) and SA@AuNPs (d) (insert graphs present DLS results).

and 854 cm^{-1} correspond to the presence of O–H/N–H vibrations, aromatic (C–H) stretch, C=O group, C=O stretching of amide I, N–H bending of amide II, C–N stretching and N–H bending of amide III, O–C–O stretching, and C–H stretching, respectively. It appears that the hydrophilic layer of AuNPs, synthesized from SA, differs from that of AuNPs obtained from gelatine/SA colloid. The FT-IR spectrum of the former completely resembles that of the SA phytochemicals, whereas the latter exhibits spectral characteristics akin to those of gelatine. The absence of significant peaks at 1155–1066 cm^{-1} indicative of O–C–O vibration[37] found in phytochemicals, distinguishes gelatine coating from phytochemical coating. Moreover, phytochemical layer, with numerous functional groups containing O–H groups, typically shows a broad peak in the high-frequency region 3856–3074 cm^{-1}. Conversely, the gelatine layer exhibits a sharp peak in this region, which is characterized by N–H vibration. Notably, the absence of a peak assigned to N–H structural vibration at the wavelength of 3300 cm^{-1} in the spectrum of gelatine/SA@AuNPs unequivocally demonstrates a robust interaction between the amine groups and AuNPs.[25]

The outcomes from TGA conducted in the temperature range of 25–800 °C provide additional confirmation of the distinction between these coatings. Accordingly, the TGA trace with DTG curve of AuNPs synthesized from gelatine/SA mixture closely mirrors that of gelatine powder (Fig. 3c), as documented in previous studies.[38,39] In which, the major weight loss observed in the temperature range of 250–450 °C is related to the decomposition of proline in gelatine. The residual events observed within the ranges of 25–250 °C and 450–800 °C are marginal and attributed to heat water and degradation of aromatic structures. Following the thermal decomposition process, the remaining residue of approximately 74.65% indicates the presence of AuNPs in the analytical sample. The thermogravimetric analysis result of AuNPs derived only from SA extract is similar to those of the biogenic metallic nanoparticles synthesized previously (Fig. 3d). Accordingly, the initial event observed at the temperature up to 150 °C refers to the evaporation of water (2.59%), while the second one between 250 and 350 °C attributed to degradation of phytochemicals such as carbohydrates, flavonoids, and phenolic acid (accounted for 14.53%). The most substantial weight loss was detected within the range of 450–600 °C, wherein the decomposition of resistant aromatic compounds occurs. Above 600 °C, a steady weight loss accounting for only about 0.2% was recorded. Following the final thermal decomposition, the remaining amount corresponding to SA@AuNPs is less than that synthesized from the gelatine/SA mixture, consisting of the result obtained from EDS analysis.

3.2. Identification of gelatine role in AuNPs synthesis

Findings from the above section prompted us to question about the respective contribution of SA extract and gelatine in the mixture to the synthesis of AuNPs, especially considering the nitrogen-containing groups of gelatine dual functionally as both a capping and reducing agent.[33] To evaluate the role of

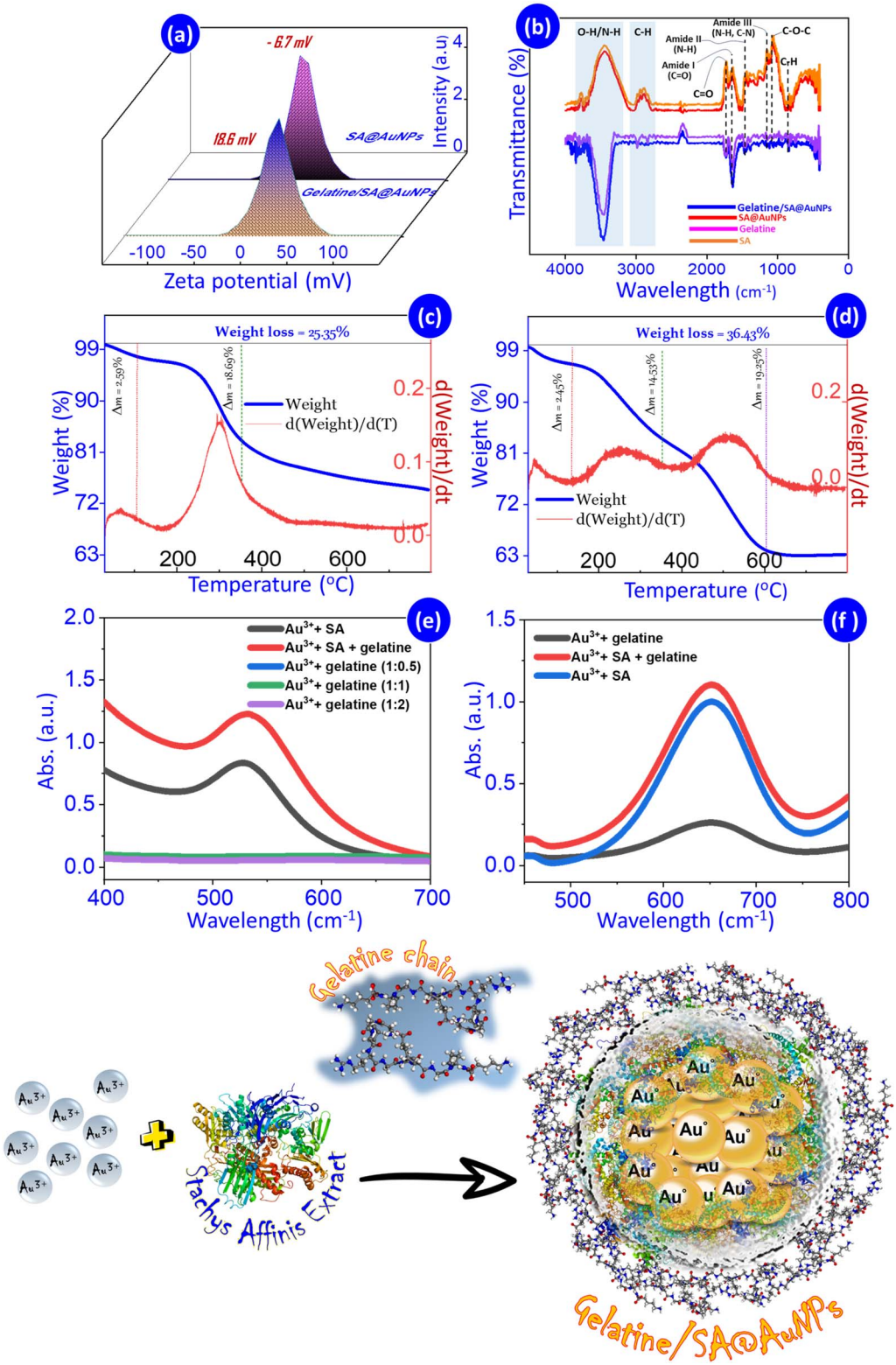

Fig. 3 Zeta potentials (a), FT-IR patterns (b), TGA-DTG curves (c) and (d), UV-vis extinction spectra (e) of as-synthesized AuNPs, and UV-vis absorption of TMB oxidation with the different prepared catalysts (f).

gelatine in our study, we conducted an analytical comparison of a surface plasmon resonance (SPR) of AuNPs formed in three reaction mixtures including Au^{3+}/gelatine, Au^{3+}/SA extract, and Au^{3+}/SA extract/gelatine. The UV-vis absorption spectra of these reaction solutions in the 400–700 nm wavelength range are illustrated in Fig. 3e. Interestingly, the reaction of Au^{3+}/gelatine

failed to result in any discernible characteristic vibrations in the absence of SA extract, even though the gelatine content was increased many times. Conversely, a pronounced resonance peak at 530 nm, a characteristic plasmon resonance band for AuNPs, was observed in the case of adding SA extract to the reaction mixture. Noticeably, the absence of gelatine in the Au^{3+}/SA extract solution results in a reduction in absorption intensity at 530 nm, albeit no discernible shift in the position of the absorption peak (Fig. S2a†). Accordingly, the particle size of nanoparticles is known to be related to both the absorption intensity and half-peak width. This experimental outcome elucidates the primary function of gelatine as a capping agent in the AuNPs phytosynthesis and simultaneously confirms the observation from SEM-EDS, and TEM analysis that adding gelatine into SA extract results in a reduction in the particle size of formed AuNPs. Overall, in the process of synthesizing AuNPs, SA extract with phytochemicals serves as a powerful reductant, facilitating the Au(III) ion reduction to form Au. Subsequently, gelatine with nitrogen-containing functional groups acts as a secondary reducing agent, contributing to encapsulation, desperation, and stabilization of the generated AuNPs. The schematic representation of AuNPs formation is provided at the end of Fig. 3.

The biogenic AuNPs along with phytochemical coating have long been recognized for their consistent and reliable peroxidase-mimicking activity. Therefore, will the coating of another layer such as gelatine impact the peroxidase-mimic property of AuNPs? This question prompted us to perform another experiment comparing the catalytic activity between SA@AuNPs and gelatine/SA@AuNPs colloids in the TMB oxidation with H_2O_2. The obtained result reveals that the catalytic activity of gelatine/SA@AuNPs colloid is even higher than that of SA@AuNPs (Fig. 3f and S2b†), suggesting its potential utility as an effective nanozyme in practical applications. Before applying this nanozyme in practice, it is crucial to ascertain its optimal synthesis conditions through the SPR analytical comparison of the colloidal nanozyme obtained under varied conditions.

3.3. Optimization of catalyst synthesis

In the pursuit of efficient and environmentally friendly methods in nanotechnology, researchers have delved into the potential of harnessing natural resources for nanoparticle synthesis. Sustainable nanoparticle production using plant extracts has emerged as a promising alternative to traditional chemical methods, offering advantages such as cost-effectiveness, environmental sustainability, and biocompatibility. The mechanism of AuNPs formation using plant extracts has been elucidated in numerous reports.[40] Additionally, it has been noted that the properties of AuNPs depend heavily on synthesis parameters such as reaction time, incubation temperature, and initial concentration of reactants.[13,41] Therefore, investigating the influence of experimental factors to identify optimal synthesis conditions is crucial for enhancing the efficiency of AuNPs synthesis.

In the exploration of the impact of Au^{3+} : SA : gelatine ratio on the AuNPs synthesis, a clearer of the individual roles played by SA extract and gelatine in this process is discernible. Specifically, if the gelatine content remains constant, alterations in the rate of Au^{3+} concentration or the reduction in the rate of SA extract result in the persistent oscillation of both SPR and λ_{max} which characterize the morphology and stability of as-synthesized AuNPs (Fig. 4a). The optimal ration of Au^{3+} to SA extract for the synthesis process was found to be 2 : 1. In particular, excessively increasing the Au^{3+} concentration results in a noticeable shift of λ_{max} peak to longer wavelengths, accompanied by a blunting of SPR peak and a rapid decrease in its intensity. These phenomena are indicative of the agglomeration occurring within the AuNPs synthesis. The analogous trend has been also observed in our previous studies[14,30,42–44] and other investigations into the biogenic AuNPs synthesis. Accordingly, the excessive elevation of Au^{3+} would lead to a depletion of the natural extract available for preventing aggregation of nanoparticles. Moreover, the excess Au^{3+} subsequently adheres to the surface of the as-synthesized nanoparticles, thereby further amplifying their propensity for agglomeration. Gelatine functions as an anti-aggregation agent rather than a reducing agent in the synthesis process, as evidenced by the optimal Au^{3+} : SA ratio of 2 : 1 observed even in the synthesis conducted in the absence of gelatine (Fig. 4b). In clearer terms, the presence of gelatine partially constrained agglomeration, resulting in the manifestation of SPR signal at Au^{3+} : SA ratio of 10 : 1 (Fig. 4c), whereas no SPR signal was observed in the presence of gelatine during synthesis (Fig. 4b). Another piece of evidence indicates that, within the optimal ratio of Au^{3+} to SA, variations in gelatine concentrations minimally shift the maximum SPR peak, but primarily influence its intensity (Fig. 4c). Increasing the rate of gelatine will inherently limit the aggregation process. However, an excessive increase in the concentration of this stabilizer raises its viscosity, which in turn reduces the diffusion rate of gold precursor (Au^{3+}) in the nucleation stage of synthesis. The longer nucleation time consequently leads to an increase in the as-synthesized AuNPs size. To reinforce this theory, a series of experiments was conducted to examine the effect of gelatine concentration on the particle size of the synthesized nanoparticles, in which the gelatine concentration was gradually increased from 1% to 7.5%. The obtained results revealed that at the gelatine concentration below 2.5%, the particle size of gelatine/SA@AuNPs is predominantly around 200 nm. Further increase in gelatine content leads to a decrease in the peak intensity of the particle size distribution curve, accompanied by a gradual shift towards larger particle sizes and broader size distributions (Fig. S3†), demonstrating a decreased stabilizing effect at higher gelatine. This finding explains why increasing the content of gelatine in the Au^{3+} : SA : gelatine ratio to 0.5 or higher results in a sharp decrease in the intensity of SPR peak. Notably, the absorption spectrum of 2 : 1 : 5 solution mixture is flat in the spectral range of 400 to 700 nm, indicating the absence of AuNPs within the solution. Thus, the optimal ratio for the biogenic AuNPs synthesis is 2 : 1 : 0.5 for Au^{3+}, SA, and gelatine, respectively.

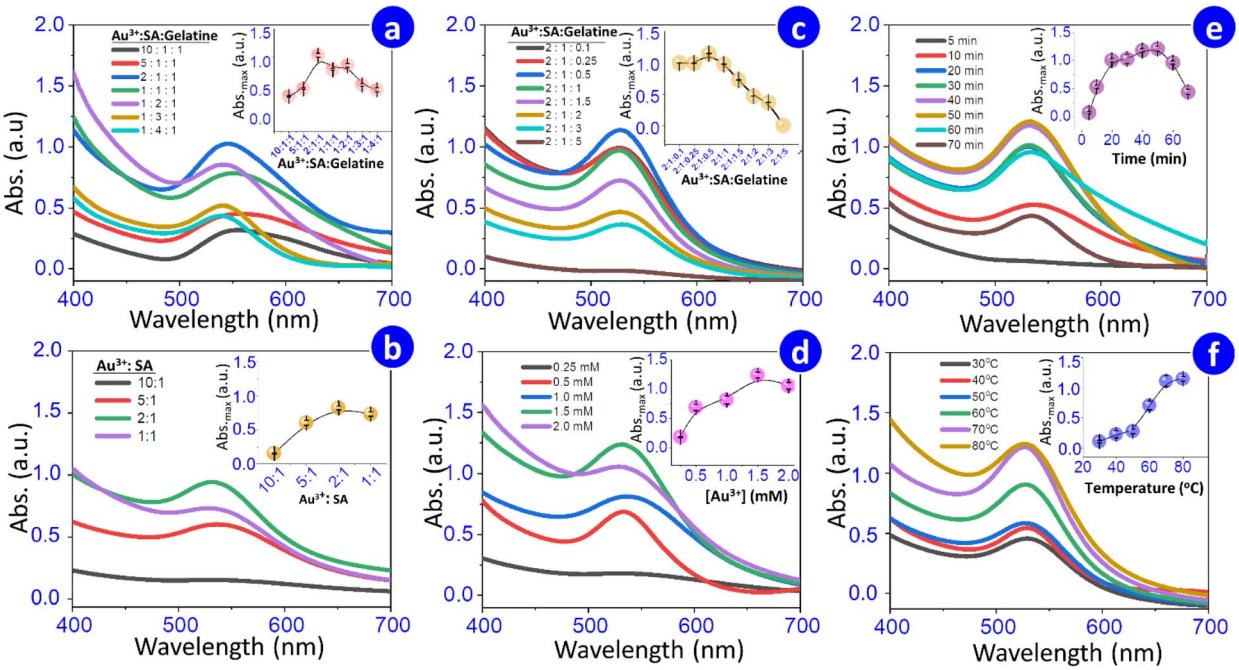

Fig. 4 UV-vis extinction spectra of gelatine/SA@AuNPs indicating the effect of reactants ratio (a) and (c), the concentration of Au precursor (d), incubation temperature (e), and temperature (f) on the synthesis process. UV-visible extinction spectra of SA@AuNPs (b).

In addition to the component ratios involved in the synthesis, reaction time, temperature, and starting concentration of the gold precursor significantly influence the AuNPs formation. As mentioned above, variations in the concentration of Au^{3+} concentrations, whether insufficient or excessive, impact both the quantity and morphology of AuNPs. Empirical evidence (Fig. 4d) demonstrates that a concentration of 1.5 mM is optimal for synthesizing the colloidal nanozyme AuNPs.

The synthesis of AuNPs from SA in the presence of gelatine is likely to follow a pathway similar to that of metal nanoparticles when utilizing natural extracts. In particular, when the reaction time is too short, the synthesis process halts at the formation of Au atoms and their nanocluster, without progressing through further stages such as nanocluster aggregation into nanoparticles. However, an excessively long synthesis time results in the agglomeration of AuNPs. This mechanism has been widely referenced in our previous[30,41,43] and in prior studies,[45] concerning the natural extract-mediated synthesis of metallic nanoparticles. Consistent with the studies just mentioned, this study observed no resonance during synthesis periods of less than 10 min (Fig. 4e). This corresponds to the nanocluster pre-aggregation stage in which gold atoms is formed through the reduction of Au^{3+} by SA extract, subsequently undergoing nucleation and aggregation to yield nanocluster. In the subsequent minutes of observation, the surface plasmon vibrations at around 530 nm showed a marked increase, likely attributed to the typical plasmon resonance band for pure AuNPs, aligned with the coalescence stage. Subsequently, the SPR intensity remained nearly constant as the nanoparticles size increased while that of polydispersity declined. Extending the synthesis duration further destabilizes the nano-system owing to the agglomeration nanoparticles, leading to a swift decline in the SPR intensity. In this study, consistent with our previous research, halting synthesis between 40 and 50 min proved optimal for producing a stable AuNPs solution.

Beyond synthesis time, the thermal factor inherently plays a crucial role in influencing the AuNPs synthesis. Raising the incubation temperature supplies additional energy to the rate-limiting stage of Au^{3+} reduction, thus enhancing the efficiency of AuNP formation. In this study, the temperature increase beyond 50 °C significantly improves the AuNPs formation. However, further increases in the incubation temperature from 70 to 80 °C only result in a slight intensity of SPR, leading to the selection of 70 °C as the optimal temperature for the synthesizing AuNPs from SA/gelatine colloid.

Optimizing the synthesis process becomes meaningless if the formed nanocomposite is unstable, which is particularly important in practice when long-term storage is required. In fact, after more than 4 months of storage, the zeta potential of gelatine/SA@AuNPs decreased only slightly from 18.6 mV to 16 mV (Fig. S4a†), and its catalytic efficiency lost by approximately 10% (Fig. S4b†), thereby confirming its durability and practical applicability. Overall, to achieve AuNPs of optimal quality, the synthesis should be conducted using an Au^{3+} concentration of 1.5 mM in the Au : SA : gelatine ratio of 2 : 1 : 0.5 at an incubation temperature of 70 °C for a duration of between 40 and 50 min.

3.4. Peroxide-like activity of gelatine/SA@AuNPs

As mentioned above, the preliminary surveys indicate that as-synthesis gelatine/SA@AuNPs exhibits significant peroxide-like activity. The coating an additional layer such as gelatine

in combine with the SA extract layer, can enhance slightly the peroxidase-mimic property of AuNPs. However, further investigation is needed to fully understand the properties of gelatine/SA@AuNPs and to establish optimal conditions for maximizing its catalytic activity. These findings will be crucial for its practical applications, particularly in colorimetric biosensors. Nobel metal nanoparticles, referred to as nanozymes, demonstrate peroxide-like activity by facilitating the oxidation of TMB through reduction reactions involving hydrogen peroxide. Specifically, the reactive oxygen radicals formed during the reduction reactions subsequently oxidize TMB, resulting in noticeable lightening of the solution colour. This colour change serves as a basis for quantifying the concentration of the analyte. Evidence suggests that the presence of gelatine/SA@AuNPs intensifies the blue colour of the reaction solution. Qualitatively, the absorption band located at 655 nm shows a marked increase upon the addition of this nanozyme (Fig. 5a). The colorimetric oxidation of TMB is strictly controlled by the catalyst quantity, concentration of colorimetric substrate, solution pH, temperature, and incubation duration. The effect of the aforementioned factors on the catalytic activity of gelatine/SA@AuNPs follows the same principles observed with other nanozymes, where an increase in these parameters can inhibit the oxidation process. Specifically, high temperature and solution pH facilitate the decomposition of H_2O_2, thereby inhibiting the progression of the chain reaction in the catalytic oxidation of TMB. Conversely, at excessively low pH, this colorimetric substrate itself decomposes readily. Experimental results indicate that optimal conditions for catalytic oxidation of TMB in the presence of gelatine/SA@AuNPs occur at a pH of 5 (Fig. 5b) and an incubation temperature of 50 °C (Fig. 5c). The used colorimetric substrate has limited solubility in an aqueous buffer, therefore, at high concentrations, TMB may precipitate at elevated concentrations during the reactions (Fig. 5d). Essentially, coating SA retains a measurable amount of natural reductants, allowing it to participate in the oxidation–reduction reaction. Consequently, an excessive concentration of gelatine/SA@AuNPs may reduce the oxidation efficiency of TMB (Fig. 5e). Therefore, to maintain the peroxide-like activity of gelatine/SA@AuNPs, the oxidation reaction should be conducted with TMB and gelatine/SA@AuNPs at recommended concentrations of at 5 mM and 60 μL, respectively.

In terms of reaction time, for conventional metal nanoparticles-based catalysts, extended incubation time results in reduced activity due to its tendency to aggregate. Conversely, for gelatine/SA@AuNPs, the presence of gelatine layer appears to prevent this agglomeration. Notably, following the attainment of its peak at 655 nm, the absorbance intensity remains nearly constant for at least an additional 1 h (Fig. 5f). This enhancement contributes to the stability and reliability of the targeted nanozymes in colorimetric assays.

H_2O_2 serves as the initiator for the catalytic oxidation of TMB, with its increased concentration accelerating the reaction efficiency. However, it is essential to establish the linear range in which catalytic efficiency increases with the H_2O_2 concentration. Defining this range enhances the reliability of gelatine/SA@AuNPs when utilized as a nanoenzyme in colorimetric assay. Eleventh concentration ranges of H_2O_2, spanning 1–1000 mM, were examined to identify this linear region (Table S3 in the ESI†). As anticipated, the catalytic efficiency of gelatine/SA@AuNPs demonstrated a linear increase across these ranges, with an *R*-squared value (R^2) consistently exceeding

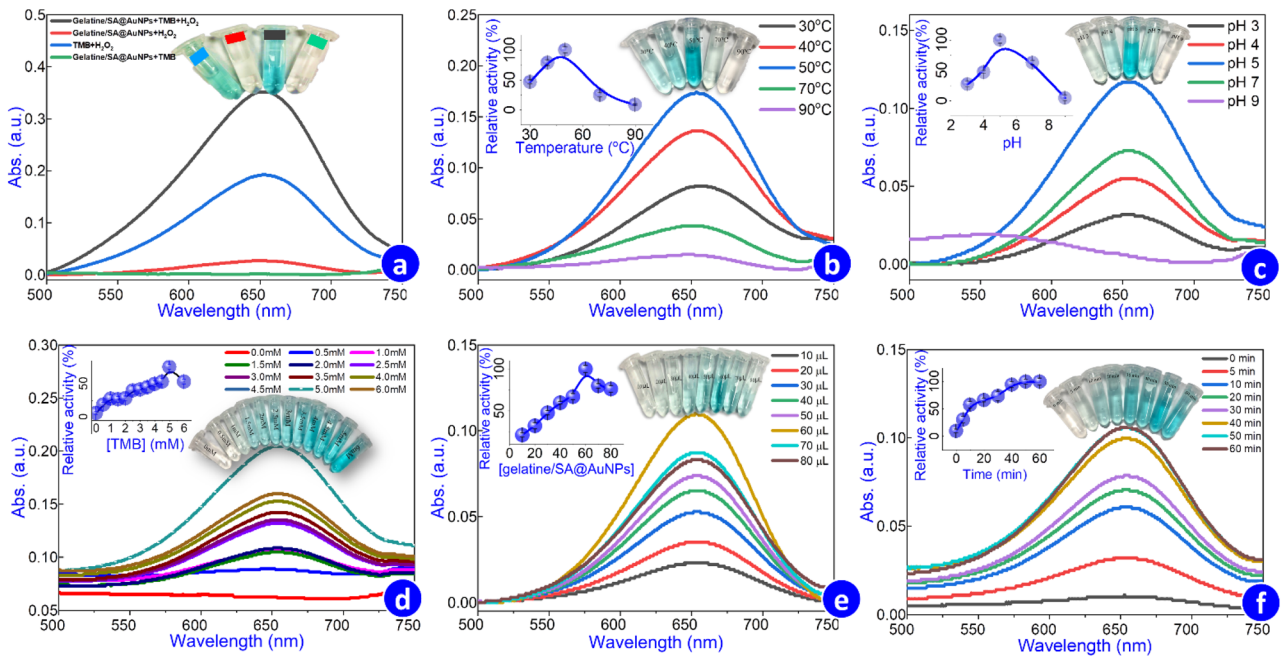

Fig. 5 UV-vis absorbance spectra of TMB solution subjected to various oxidation conditions (a); the effects of incubation temperature (b), buffer solution pH (c), initial concentration of TMB (d), catalyst amount (e), and reaction time (f) on these spectra.

0.978. A notable observation is the maximum R^2 value of 0.9963, which was recorded for the H_2O_2 concentration range of 10–800 μM, with the regression equation: Abs. = 0.0012 [H_2O_2] + 0.1244. The steady-state kinetic analysis, using the Michalis–Menten equation under the optimal conditions for TMB oxidation (Fig. S5†), reveals that the calculated Michalis–Menten constant (K_m) for H_2O_2 is exceptionally low (K_m = 0.056), which is 66 times lower compared to the natural horseradish peroxidase enzyme and significantly lower than most previously synthesized AuNPs (Table S4†). This low K_m is critical for evaluating the interaction of nanozyme with H_2O_2. The low value of K_m suggests that gelatine/SA@AuNPs exhibits a strong affinity for H_2O_2, a significant factor in the catalytic oxidation reaction, as the interaction between catalyst and H_2O_2 is essential for producing reactive oxygen species directly involved in the TMB oxidation. Furthermore, the low K_m constant indicates that gelatine/SA@AuNPs can achieve optimal catalytic activity even at low H_2O_2 concentrations, enhancing its reliability in the colorimetric analysis. The unusually strong affinity of the targeted catalyst with H_2O_2, relative to other biogenic AuNPs, may be attributed to its coating with the gelatine layer. Given its outstanding catalytic properties, gelatine/SA@AuNPs is expected to provide robust reliability in detecting cholesterol specifically, and in colorimetric assay generally.

3.5. Cholesterol detection in the presence of gelatine/SA@AuNPs

The conventional colorimetric method for determining cholesterol is based on its easy oxidation by dissolved oxygen, facilitated by ChOx, resulting in the generation of a small amount of H_2O_2. The H_2O_2 produced then oxidizes TMB, leading to a colour change in the test solution. The absorption spectrum of the TMB-containing solution, following catalytic oxidation, increases proportionally with rising cholesterol concentration, enabling accurate its quantification. A typical nanoparticle of noble metal is added to accelerate colour development in the reaction solution, enhancing the reliability of the colorimetric measurement. Due to its high catalytic activity at low H_2O_2 concentrations, gelatine/SA@AuNPs is particularly well-suited for use in the determination of cholesterol.

The survey results reveal that at cholesterol concentrations below 1000 μM, the accuracy of its colorimetric quantification in the presence of gelatine/SA@AuNPs is very high. The linear relationship between cholesterol concentration and intensity of ox-TMB within this range demonstrates an R^2 exceeding 0.996. Using gelatine/SA@AuNPs, cholesterol can therefore be colorimetrically quantified across a large concentration range. Notably, increasing the cholesterol concentration in the test solution to 2000 μM markedly reduces reliability, as evidenced by a lower R^2 coefficient. The equation derived from linear regression for cholesterol concentrations between 10 and 1000 μM is Abs. = 0.0005 [cholesterol] − 0.0013, with a correlation coefficient of 0.997 (Fig. 6a). The limit of detection (LOD) was found to be around 3.48 μM (Table S5†), marking it as one of the lowest values observed for colorimetric cholesterol detection compared to other AuNP-based catalyst types reported in previous studies (Table S6†). The results obtained above provide a significant foundation for evaluating the potential application of gelatine/SA@AuNPs in practical cholesterol quantification.

3.6. Practical cholesterol quantification

One of the inherent problems of quantitative methods in the nutrition field is the interference from coexisting substances in food. In reality, numerous other substances are often accompanied by cholesterol in food we consume daily, including various inorganic and organic compounds such as $ZnCl_2$, $MgCl_2$, niacin, vitamins, tryptophane, glycine, uric acid, and glucose. The aforementioned compounds, along with cholesterol, are commonly present in highly nutritious foods like meat, fish, milk, snacks, and biscuits. Fundamentally, such compounds are unreactive with cholesterol, but ChOx can interact with them. If this interaction is substantial, it could potentially impact the accuracy of the quantitative measurements. Consequently, it is essential to assess the ChOx specificity for cholesterol in comparison to these coexisting substances. To clearly evaluate the enzyme's specificity of colorimetric assay in the presence of the targeted catalyst, the concentration of these substances is set to be ten times greater than that of cholesterol. The results indicated that the presence of these compounds, even at high concentrations, had minimal impact on the colour intensity of the colorimetric system based on TMB/gelatine/SA@AuNPs/ChOx (Fig. 6b). Arguably, the selective detection of cholesterol in the investigated assay is primarily attributed to the high substrate specificity of ChOx, which exclusively catalyzes the cholesterol oxidation, leading to the H_2O_2 production. The generated H_2O_2 subsequently triggers a color change in TMB solution through the gelatine/SA@AuNPs-assisted oxidation reaction, as described in Fig. 1b. Other coexisting substances such as the amino acids, the mineral salts, or glucose do not undergo oxidation by ChOx, and thus do not generate H_2O_2, leading to negligible influence on the assay output. This result further enhances the reliability of colorimetric cholesterol quantification using gelatine/SA@AuNPs.

Snack and convenience foods, such as butter and pork floss baguette, are popular foods among young people worldwide, including in Vietnam. However, excessive consumption of these fast foods has been identified as a significant risk factor for obesity today.[46,47] Therefore, snack ticks and butter & pork floss baguette are the primary objectives of our investigation for cholesterol content analysis using the colorimetric assay, with gelatine/SA@AuNPs serving as a new catalytic agent. To enhance the reliability and accuracy of the obtained measurements, we applied both direct determination and spike-and-recovery methods to quantify cholesterol in these fast foods. The analysis revealed that cholesterol concentrations in the snack and baguette samples were 95.5 and 66.10 mg kg^{-1}, respectively, with a recovery efficiency ranging from 91.42 to 109.119% (detailed descriptions presented in Table S7†), meeting the criteria outlined in AOAC Appendix F. High recovery efficiency across multiple concentration levels

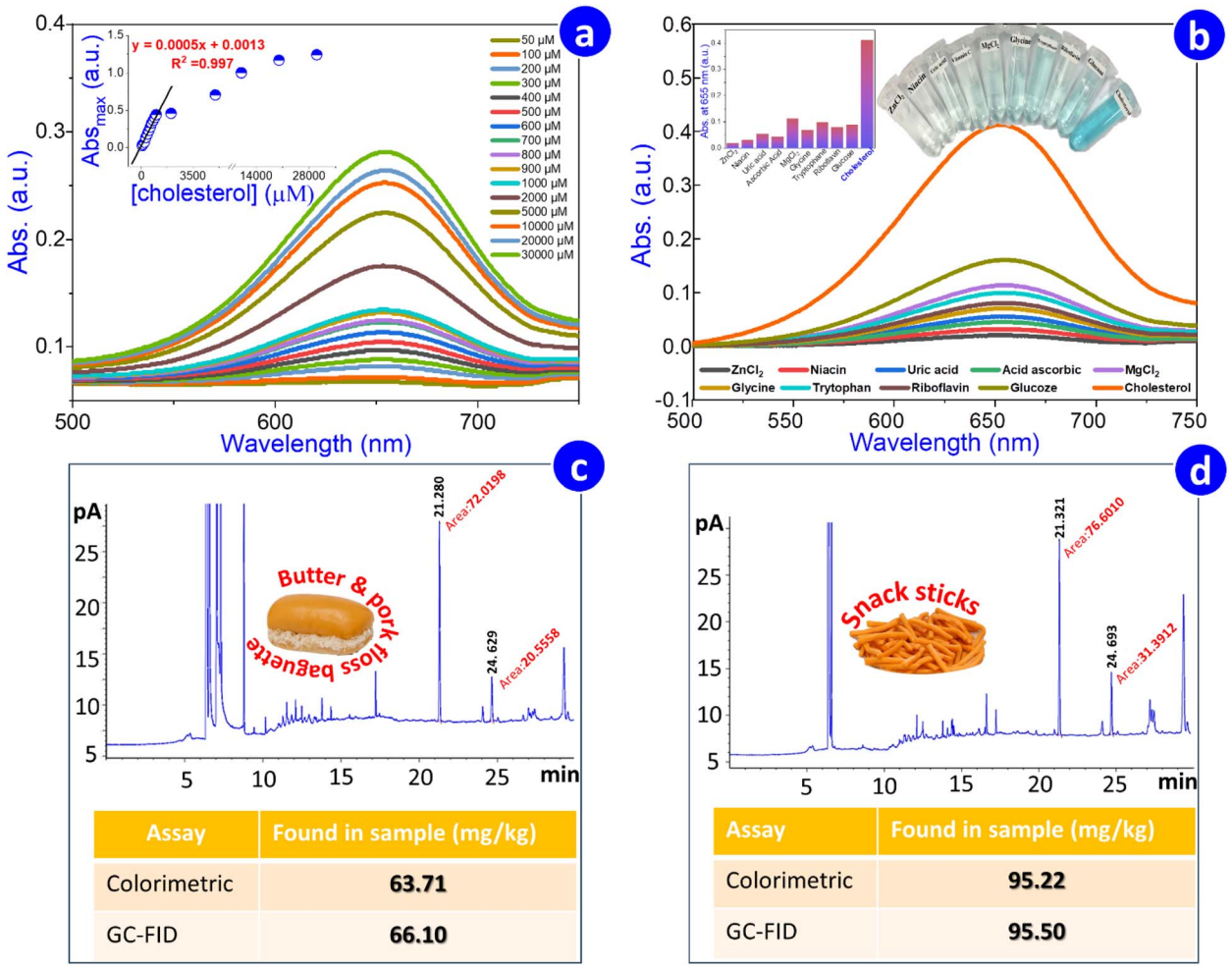

Fig. 6 UV-vis absorbance spectra of oxidized TMB solution as a function of cholesterol concentration (a) and added interferents (b), GC-FID chromatogram of baguette (c) and snack samples (d) as well as comparative analysis of cholesterol content in these samples.

indicates that this colorimetric quantification is suitable for use with the tested sample and minimally affected by the sample matrix. To verify the accuracy of the newly obtained results, the samples of snack and baguette were sent to a third-party – "Eurofinds Scientific" for quantification of cholesterol content using GC-FID with samples ID of 743-2023-00003334 and 743-2023-00009031, respectively. The analysis reports (in Vietnamese) are provided in detail within the ESI (Fig. S6†). The obtained results met our expectations, indicating that the cholesterol contents in snack and baguette, as determined by colorimetric assay using gelatine/SA@AuNPs and GC-FID measurement, were closely consistent (Fig. 6c and d), with only deviations of 0.29% for snack sticks and 3.61% for butter & pork floss baguette.

4. Conclusion

Although gelatine possesses reducing capabilities, in the synthesis of biogenic AuNPs in the presence of SA extract, it primarily acts as an anti-agglomeration agent, forming an outer shell around the biogenic AuNPs, effectively mitigating aggregation. Moreover, the coating of gelatine does not impede the catalytic activity of biogenic AuNPs; instead, it slightly enhances its inherent catalytic performance. Importantly, this coating does not interfere with the practical applications of AuNPs. The colorimetric quantification of cholesterol, supported by the biogenic AuNPs coated with gelatine, demonstrates high reliability and accuracy. With its well-defined composition and properties, the incorporation of gelatine during the synthesis process appears to be the most effective solution currently available to minimize agglomeration – a significant challenge in the synthesis and production of nanozymes. More importantly, the properties and morphology of the metallic nanoparticles can be precisely controlled by indirectly influencing gelatine, a hypothesis that requires further validation. In addition to gelatine, various other stabilizing agent should be investigated to optimize the synthesis process and enhance control over metallic nanoparticle production.

Data availability

The data are included within the article.

Author contributions

Thi Lan Huong Nguyen: project administration. Ngoc Vy Nguyen: methodology, software. Van-Dat Doan: project administration, supervision, methodology, review & editing. Thi Dung Nguyen: methodology, experiments, validation. Anh-Tien Nguyen: methodology, experiments, validation. Thi Long Do: methodology, experiments, validation. Renat Maratovich Akhmadullin: methodology, validation. Hien Y Hoang: writing – original draft, writing – review & editing, supervision, software, data curation, validation.

Conflicts of interest

The authors have no conflicts of interest to declare. All co-authors have seen and agree with the contents of the manuscript and there is no financial interest to report.

References

1 M. Cao, C. Huang, Y. Zhang, X. Yang, L. Cui, A. Li, J. Xu and J. Liu, *Sens. Actuators, B*, 2024, **404**, 135235.
2 W. Zheng, B. Han, Y. n. Zhang, L. Liu and Y. Zhao, *Anal. Chim. Acta*, 2024, **1287**, 342043.
3 L. H. Li, E. P. Dutkiewicz, Y. C. Huang, H. B. Zhou and C. C. Hsu, *J. Food Drug Anal.*, 2019, **27**, 375–386.
4 A. Ndhlala, A. Kavaz Yüksel, N. Çelebi and H. Doğan, *Foods*, 2023, **12**, 4424.
5 H. Abed, R. Sabouni and M. Ghommem, *RSC Adv.*, 2024, **14**, 39472–39497.
6 M. Ameen Sha, P. C. Meenu, H. Haspel and Z. Kónya, *RSC Adv.*, 2024, **14**, 24561–24573.
7 B. Kuswandi and M. A. Hidayat, in *Low-cost Diagnostics*, Royal Society of Chemistry, 2024, pp. 1–22.
8 S. Bhandari, V. S. Parihar, M. Kellomäki and M. Mahato, *RSC Adv.*, 2024, **14**, 28844–28853.
9 S. Malik, J. Singh, K. Saini, V. Chaudhary, A. Umar, A. A. Ibrahim, S. Akbar and S. Baskoutas, *Anal. Methods*, 2024, **16**, 2777–2809.
10 J. Yang, X. Shu, S. Qin, L. Huang, S. Cheng and Y. Wang, *Microchem. J.*, 2024, **197**, 109883.
11 C. Mu, D. Feng, M. Khan, H. Song, S. Munir, Q. Hu and L. Yu, *Anal. Chem.*, 2025, **97**, 3926–3936.
12 K. A. Altammar, *Front. Microbiol.*, 2023, **14**, 1155622.
13 T. H. A. Nguyen, V.-C. Nguyen, T. N. H. Phan, V. T. Le, Y. Vasseghian, M. A. Trubitsyn, A.-T. Nguyen, T. P. Chau and V.-D. Doan, *Chemosphere*, 2022, **287**, 132271.
14 T. H. A. Nguyen, V. T. M. Nguyen, V. T. Le, V.-D. Doan, T. P. Chau, V. C. Nguyen, A.-T. Nguyen and Y. Vasseghian, *Mater. Lett.*, 2022, **309**, 131307.
15 T. Khan, N. Ullah, M. A. Khan, Z.-R. Mashwani and A. Nadhman, *Adv. Colloid Interface Sci.*, 2019, **272**, 102017.
16 H. Guan, Y. Song, B. Han, D. Gong and N. Zhang, *Spectrochim. Acta, Part A*, 2020, **241**, 118675.
17 X. Zhang, M. Wei, B. Lv, Y. Liu, X. Liu and W. Wei, *RSC Adv.*, 2016, **6**, 35001–35007.
18 M. Alle, R. Bandi, G. Sharma, R. Dadigala, S.-H. Lee and J.-C. Kim, *Int. J. Biol. Macromol.*, 2022, **201**, 686–697.
19 T. L. H. Nguyen, V.-D. Doan, Q.-H. Tran, A. T. Nguyen, V. A. Tran, V. T. Le, A. Renat Maratovich and H. Y. Hoang, *Microchem. J.*, 2024, **200**, 110343.
20 N. H. Anh, M. Q. Doan, N. X. Dinh, T. Q. Huy, D. Q. Tri, L. T. Ngoc Loan, B. Van Hao and A.-T. Le, *RSC Adv.*, 2022, **12**, 10950–10988.
21 A. A. Kajani, A.-K. Bordbar, S. H. Zarkesh Esfahani and A. Razmjou, *RSC Adv.*, 2016, **6**, 63973–63983.
22 V. T. Le, T. G. Duong, V. T. Le, T. L. Phan, T. L. Huong Nguyen, T. P. Chau and V.-D. Doan, *RSC Adv.*, 2021, **11**, 15438–15448.
23 A. Pourjavadi and R. Soleyman, *J. Nanopart. Res.*, 2011, **13**, 4647–4658.
24 B. P. Vinjamuri, K. Papachrisanthou, R. V. Haware and M. B. Chougule, *J. Drug Delivery Sci. Technol.*, 2021, **63**, 102423.
25 M. P. Neupane, S. J. Lee, I. S. Park, M. H. Lee, T. S. Bae, Y. Kuboki, M. Uo and F. Watari, *J. Nanopart. Res.*, 2011, **13**, 491–498.
26 I.-H. Chen, Y.-F. Chen, J.-H. Liou, J.-T. Lai, C.-C. Hsu, N.-Y. Wang and J.-S. Jan, *Mater. Sci. Eng., C*, 2019, **105**, 110101.
27 J.-J. Zhang, M.-M. Gu, T.-T. Zheng and J.-J. Zhu, *Anal. Chem.*, 2009, **81**, 6641–6648.
28 Y. Liu, X. Liu and X. Wang, *Nanoscale Res. Lett.*, 2010, **6**, 22.
29 Q. K. Vo, M. N. N. Thi, P. P. N. Thi and D. T. Nguyen, *Processes*, 2019, **7**, 631.
30 T. L. H. Nguyen, V. Thuan Le, M. A. Trubitsyn, V. D. Doan, P. H. Dang, A. T. Nguyen, H. Thai Le, T. H. Nguyen and H. Y. Hoang, *Biochem. Eng. J.*, 2024, **207**, 109335.
31 A. Venditti, C. Frezza, D. Celona, A. Bianco, M. Serafini, K. Cianfaglione, D. Fiorini, S. Ferraro, F. Maggi, A. R. Lizzi and G. Celenza, *Food Chem.*, 2017, **221**, 473–481.
32 A. Hayat, W. Haider, Y. Raza and J. L. Marty, *Talanta*, 2015, **143**, 157–161.
33 A. L. Siegel and G. A. Baker, *Nanoscale Adv.*, 2021, **3**, 3980–4004.
34 C. E. A. Botteon, L. B. Silva, G. V. Ccana-Ccapatinta, T. S. Silva, S. R. Ambrosio, R. C. S. Veneziani, J. K. Bastos and P. D. Marcato, *Sci. Rep.*, 2021, **11**, 1974.
35 S. Ghosh, S. Patil, M. Ahire, R. Kitture, D. D. Gurav, A. M. Jabgunde, S. Kale, K. Pardesi, V. Shinde, J. Bellare, D. D. Dhavale and B. A. Chopade, *J. Nanobiotechnol.*, 2012, **10**, 17.
36 D. Philip, *Spectrochim. Acta, Part A*, 2010, **77**, 807–810.
37 K. I. Hadjiivanov, D. A. Panayotov, M. Y. Mihaylov, E. Z. Ivanova, K. K. Chakarova, S. M. Andonova and N. L. Drenchev, *Chem. Rev.*, 2021, **121**, 1286–1424.
38 S. Frazier, A. Aday and W. Srubar, *Molecules*, 2018, **23**, 1121.
39 E. Biazar and S. H. Keshel, *Int. J. Polym. Mater. Polym. Biomater.*, 2014, **63**, 741–752.
40 M. A. R. Khan, M. S. Al Mamun, M. A. Habib, A. B. M. N. Islam, M. Mahiuddin, K. M. R. Karim, J. Naime, P. Saha, S. K. Dey and M. H. Ara, *Results Chem.*, 2022, **4**, 100478.

41 V.-D. Doan, B.-A. Huynh, T.-D. Nguyen, X.-T. Cao, V.-C. Nguyen, T. L.-H. Nguyen, H. T. Nguyen and V. T. Le, *J. Nanomater.*, 2020, **2020**, 1–18.
42 B. A. Huynh, V.-D. Doan, V. C. Nguyen, A.-T. Nguyen and V. T. Le, *RSC Adv.*, 2022, **12**, 27116–27124.
43 T. H. A. Nguyen, T. T. V. Le, B. A. Huynh, N. V. Nguyen, V. T. Le, V.-D. Doan, V. A. Tran, A.-T. Nguyen, X. T. Cao and Y. Vasseghian, *Environ. Res.*, 2022, **212**, 113281.
44 V. D. Doan, B. A. Huynh, T. D. Nguyen, X. T. Cao, V. C. Nguyen, T. L. H. Nguyen, H. T. Nguyen and V. T. Le, *J. Nanomater.*, 2020, **2020**, 1–18.
45 J. Polte, T. T. Ahner, F. Delissen, S. Sokolov, F. Emmerling, A. F. Thünemann and R. Kraehnert, *J. Am. Chem. Soc.*, 2010, **132**, 1296–1301.
46 V. Y. Njike, T. M. Smith, O. Shuval, K. Shuval, I. Edshteyn, V. Kalantari and A. L. Yaroch, *Adv. Nutr.*, 2016, **7**, 866–878.
47 A. Skoczek-Rubińska and J. Bajerska, *Nutr. Res.*, 2021, **96**, 20–36.